Lab on a Chip

PAPER

View Article Online
View Journal | View Issue

Cite this: *Lab Chip*, 2014, **14**, 1785

Three-dimensional, sharp-tipped electrodes concentrate applied fields to enable direct electrical release of intact biomarkers from cells

Mahla Poudineh,[a] Reza M. Mohamadi,[b] Andrew Sage,[b] Laili Mahmoudian,[b] Edward H. Sargent*[a] and Shana O. Kelley*[bc]

Received 3rd February 2014,
Accepted 23rd March 2014

DOI: 10.1039/c4lc00144c

www.rsc.org/loc

Biomarkers such as proteins and nucleic acids released from human cells, bacteria, and viruses offer a wealth of information pertinent to diagnosis and treatment ranging from cancer to infectious disease. The release of these molecules from within cells is a crucial step in biomarker analysis. Here we show that purely electric-field-driven lysis can be achieved, inline, within a microfluidic channel; that it can produce highly efficient lysis and biomarker release; and, further, that it can do so with minimal degradation of the released biomarkers. Central to this new technology is the use of three-dimensional sharp-tipped electrodes (3DSTEs) in lysis, which we prove using experiment and finite-element modeling produce the electric field concentration necessary for efficient cell wall rupture.

Introduction

Biomarkers including nucleic acids, proteins, and small molecules provide information relevant to the detection and diagnosis of disease. Much effort has been put towards the realization of devices for automated molecular diagnostics that are miniaturized, cost effective, and operable at the point-of-care.[1,2] In particular, progress in microfluidics has enabled both automation and also the handling of very small volumes, enabling integration of sample preparation and biosensing functions, and obviating reliance on expert technicians and laboratory facilities.[3–6]

The release of biomarkers from the interior of a cell represents a key step in biomarker analysis. This is typically performed by lysing or permeabilizing the cell membrane.[5] On-chip cell lysis strategies include chemical, thermal, mechanical, electrochemical, and electrical methods that compromise membranes. One highly effective means of cell rupture is electrochemical lysis, where application of an electric field leads to hydrolysis of H_2O and concomitant production of hydroxyl radicals as well as hypochlorite ions in chloride-containing buffers.[6] While this approach facilitates cell membrane rupture, it may also degrade the biological molecules that are detection targets.[7] Specifically, the alkaline environment and the by-products of electrolysis at the anode degrade RNA and can negatively affect downstream analysis.[8,9] Since RNA is an important biomarker for disease diagnosis, development of techniques to efficiently release RNA that is of sufficient quantity, purity, and integrity from cells is an important goal.[4,10] With the goal of overcoming these limitations of electrochemical lysis, we focus herein on the development of a device that seeks to facilitate purely electrical lysis. Here, the goal is rapid rupture of prokaryotic cell walls accompanied by the preservation of the intracellular components with minimal negative effects on subsequent analytical analysis.[5,11]

Electrical lysis proceeds *via* electroporation, where the application of the electric field transiently produces small pores in the cell membrane. A drawback of electrical lysis has historically been the need for a high electric field (*e.g.* 10 kV cm^{-1}), which typically implies the use of high bias voltage.[12] To address the electric field requirement, Wang *et al.*[13] took advantage of a geometry modification that locally amplified the electrical field; however, the required voltage was still high (500 V), and the applied DC voltage in solution hydrolysed water and thereby created a high concentration of hydroxyl radicals. The application of an alternating current (AC) voltage offers an avenue to purely electrical lysis, since water electrolysis can be decreased under rapidly-modulated electrical field.[14] Previously-reported microfluidic systems for electrical lysis have employed frequencies in the range of 10 kHz; however, these systems suffered low throughput.[11,14] Further, at these low frequencies, the pulse duration remains sufficient to electrolyze the water and create unwanted hydroxyl radicals and other byproducts that degrade RNA.

[a] *Department of Electrical and Computer Engineering, University of Toronto, Toronto, ON, M5S 3G4, Canada. E-mail: ted.sargent@utoronto.ca*
[b] *Department of Pharmaceutical Science, Leslie Dan Faculty of Pharmacy, University of Toronto, Toronto, ON, M5S 3G4, Canada. E-mail: shana.kelley@utoronto.ca*
[c] *Department of Biochemistry, Faculty of Medicine, University of Toronto, Toronto, ON, M5S 3M2, Canada. E-mail: shana.kelley@utoronto.ca*

Here, we describe an approach to purely electrical, high-throughput lysis with the goal of retaining high quality RNA. We hypothesized that if we could generate three-dimensional structures with very sharp, extended features, then we could generate a high field at lower applied potentials than used previously. Metal electrodeposition is an ideal approach to generate such structures. A significant body of prior work[15–21] has shown that metal electrodeposition is a highly tunable process that can be used to generate structures on many different length scales. We used electrodeposition to generate arrays of large structures with sharp, extended features within a channel, and used these structures in conjunction with high AC modulation frequencies to prevent electrolysis. This approach was shown to produce efficient bacterial lysis. When planar electrodes are employed, they fail to produce biomarker release, highlighting the need for three-dimensional structures to generate a high field. We found that only by employing three-dimensional, sharp-tipped electrodes (3DSTEs), readily fabricated by bottom-up growth *via* electrodeposition, were we able to achieve the combination of acceptable driving voltages, efficient biomarker release, and preservation of RNA quality. We feature the 3DSTEs in a microfluidic platform and fabricate a high-throughput flow-through device for the front-end processing of cells and bacteria for bioanalysis. Using 3DSTEs in multiple parallel microfluidic channels, we process a millilitre sample in under 20 minutes. The feasibility of this method in microfluidic channels will allow for automation and integration of the lysis with downstream on-chip sensing.

Materials and methods

A. Bacterial preparation

E. coli (Invitrogen, Carslbad, CA) was cultured in an LB Miller medium in an incubating shaker at 37 °C for 14 hours. Prior to experimentation, the growth medium was replaced with 1× PBS. To assess the bacterial concentrations, optical absorption was measured at 600 nm.

B. Chip fabrication

Glass substrates obtained from Telic Company (Valencia, CA) were used to fabricate lysis chips. A 5 nm Cr (adhesion layer) followed by a 50 nm Au were sputtered on to the glass substrate. A top-coat of positive photoresist (AZ1600) was used. Contact lithography was used to pattern the interdigitated electrodes; the width and distance between electrodes were both equal to 50 μm. These electrodes were used as substrate for electrodeposition of gold structures. After exposing for 10 seconds, photoresist was developed. This was followed by Au and Cr wet etching and removal of the top resist. A negative photoresist, SU-8 2002 (Microchem, Newton, MA), was spin-cast at 4000 r.p.m for 40 seconds to create the apertures for electrodeposition. Line apertures (W = 5 μm) were imaged into the interdigitated electrodes covered by SU-8. To fabricate the lysis chamber, a thick SU-8 layer (3025) was spin-cast at 2000 r.p.m for 40 seconds. The final thickness of the SU-8 layer was 40 μm. Lastly, the chamber mask was imaged on the surface and the two SU-8 layers were developed using SU-8 developer for 5 minutes.

C. 3DSTE Fabrication

After dicing, chips were washed with acetone, IPA and dH$_2$O, and etched in O_2 plasma using Samco-RIE-1C reactive ion etcher at 75 W for 60 seconds to clean the surface completely. The structured electrodes were fabricated by electroplating using a standard 3 electrodes system with Ag/AgCl as the reference electrode, a platinum auxiliary electrode and the 5 μm line gold aperture as the working electrode. The working solution was 50 mM $HAuCl_4$ and 0.5 M HCl and electrodes were electrodeposited for 100 seconds at 0 mV.

D. Chip assembly

After electrodeposition, chips were washed again using dH$_2$O and etched in O_2 plasma to make a hydrophilic surface for subsequent covering with polydimethylsiloxane (PDMS). PDMS was used as a lid to cover the lysis chamber. In PDMS layer, holes were punched as inlet and outlet.

E. Flow cytometry

Following lysis, samples were incubated with propidium iodide at concentration of 25 μg mL^{-1} for 30 minutes in the dark. After incubation, samples were injected into a BD FACS Canto flow cytometer and measurements were plotted as histograms of fluorescence intensity.

F. RNA Integrity Number (RIN) measurement

The integrity of RNA was assessed at TCAG Microarray Facility of The Hospital for Sick Children (HSC) by analysing a 1 μL aliquot using a RNA6000 Nano Lab Chip on an Agilent 2100 bioanalyzer. The RIN calculation software was applied to the fluorescence profiles after separation of RNA by capillary electrophoresis, and RIN values were calculated on a scale of 1–10 (low to high RNA integrity) for each sample.

G. Quantitative reverse transcription-polymerase chain reaction (qPCR)

Five *E. coil*-specific reference genes polA (gene for *E. coli* DNA polymerase I), polB (gene for *E. coli* DNA polymerase II), GAPDH (D-glyceraldehyde-3-phosphate dehydrogenase), CycG (uroporphyrin III C-methyltransferase) and rpoB (RNA polymerase β) were selected to test the efficiency of RNA obtained from electrochemical and electrical lysis devices. Table 1 shows the names and sequences of primers selected for the experiment.

RNA was extracted from electrically and electrochemically-lysed samples using an RNeasy mini kit (Qiagen). For synthesis of cDNA from electrically and electrochemically lysed samples, an equal amount of total RNA was used (10.8 ng total

Table 1 Sequences of primers used for quantitative real time PCR

Target	Primer	Sequence (5′ to 3′)	References
polA	polA-F	ATGGTTCAGATCCCCCAA	22
	polA-R	TTCTACGCCAGAAACCGCCA	22
polB	polB-F	TGGCATCGTCGATCACCAT	22
	polB-R	TGGTTGGCATCAGAAAACGGC	22
GAPDH	GAPDH-F	TTCCGTGCTGCTCAGAAA	22
	GAPDH-R	TGTGTTTACGAGCAGTTT	22
rpoB	rpoB-F	TGAGCCAGTCTGGTCACAAGC	23
	rpoB-R	CTCGAACAGGCTTTCCGCTG	23
CysG	CysG-F	TTGTCGGCGGTGGTGATGTC	24
	CysG-R	ATGCGGTGAACTGTGGAATAAACG	24

RNA in 20 μL of RT reaction). Reverse transcription (RT) was performed using high capacity cDNA reverse transcription kit from Applied Biosystems. Q-PCR reactions were performed on an Applied Biosystems 7500 machine using Ssofast Eva Green Supermix. Briefly, 1 μL of cDNA and 500 nM of gene primers were used in a total volume of 20 μL. Conditions used for qPCR included an initial step of 2 minutes at 50 °C followed by 30 seconds at 95 °C and 40 cycles of 5 seconds at 95 °C and 30 seconds at 60 °C. A no-template negative control was included for each sample tested.

Results and discussion

We depict our device concept in Fig. 1. The sample to be processed flows over and between the 3DSTEs used to apply an electric field with the goal of biomarker release (Fig. 1A). A thick insulating photoresist (SU-8) serves as a spacer to define the vertical height of the channel. A thin chromium adhesion layer ensures reliable adhesion of Au to the surface of the glass chip. This Au layer serves as a site for gold electrodeposition and the growth of 3DSTEs. Similar structures were previously developed and used as electrochemical sensors for nucleic acids,[12,23,25–31] proteins,[32,33] and small molecules,[34] where the generated high surface areas facilitated ultrasensitive detection. Here, it is the sharp features of these structure that are attractive, coupled with a bottom-up fabrication strategy that permits large structures to be arrayed across the flow path of a fluidic channel. The dimensions of the channel accommodate flow rates as high as 100 μL min^{-1}, excellent throughput even for large-volume samples such as blood, where typical patient samples are in the range 5–10 mL.

The 3DSTEs are visualized using SEM as shown in Fig. 1C. The structures are electrodeposited from a solution of gold ions. Electrodeposition growth conditions (see Methods) were selected: i) to ensure that the 3DSTEs were as tall as they were wide (20–40 μm) to maximize reach into the solution being processed, and ii) to maximize the sharpness (minimize the radius of curvature) of the 3DSTE tips.

We turned to a combination of modelling and experiments (Fig. 2 and 3) to evaluate whether the 3DSTEs could dramatically lower the voltage required for biomarker release. The transmembrane potential is the key figure that determines whether membrane electroporation will occur, with 1 V being the typical estimated threshold for electroporation of bacterial cell walls. The dependence of the transmembrane

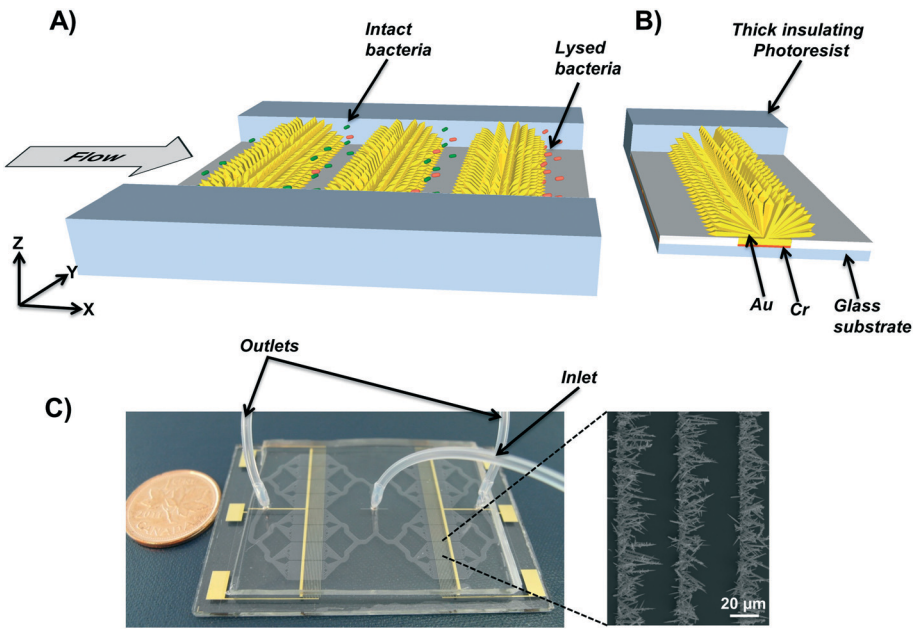

Fig. 1 Device architecture for electrical lysis study. A) Three-dimensional, sharp-tipped electrodes arrayed within a microfluidic channel. Bacteria are lysed electrically when they flow through a channel and pass between structured electrodes. B) Schematic of device cross-section. C) Image of lysis device (left), with multiple parallel channels that were used to increase the throughput of the device with two outlets. Scanning electron microscopy image (right) of electrodeposited structured electrodes.

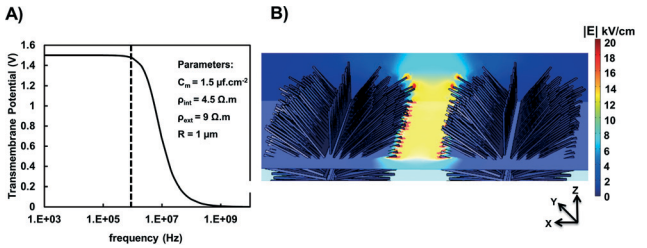

Fig. 2 Modeling electrical fields produced at sharp-tipped electrodes. A) Modeling of transmembrane potential (TMP) of bacteria caused by electrical field of 10 kV cm^{-1}. For frequencies higher than 1 MHz, TMP drops dramatically. B) Electrical field distribution at voltage V = 40 V (corresponding to the maximum for an AC voltage of 80 V_{pp}). Regions shown in red represent high field density and regions in blue show low field density.

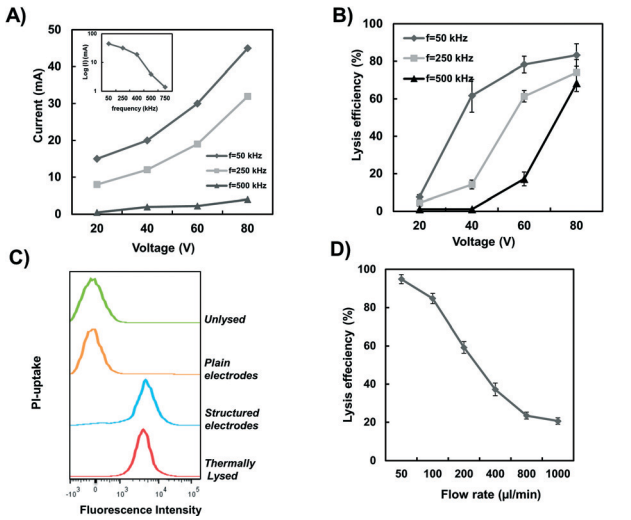

Fig. 3 Identification of conditions causing electrical *versus* electrochemical lysis. A) Current *versus* voltage at different frequencies (50 kHz, 250 kHz, and 500 kHz). A lowered current indicates a reduced rate of electrochemical reactions. The inset shows currents generated when voltage was held constant at 80 V and the frequency was varied. B) Lysis efficiency *versus* voltage at different frequencies. At low frequency and low voltages, the lysis mechanism is electrochemical while at high frequency and high voltage, it is promoted by the electrical field. C) Flow cytometry measurements of cells that were unlysed (green), plain (orange) or structured (blue) electrodes, or thermally lysed (red). The conditions for electrical lysis are f = 500 kHz, V_{pp} = 80 V, and lysis/flow rate = 1600 cell s^{-1} or 50 μl min^{-1}. D) Electrical lysis efficiency at different flow rates.

potential on modulation frequency and the cell's properties can be calculated with the expression:[11,12,14]

$$\Delta\varphi = 1.5\, RE_0 \cos\theta/(1 + (2\pi f\tau)^2)^{1/2} \quad (1)$$

where τ is

$$\tau = RC_m\left(\rho_{int} + \frac{\rho_{ext}}{2}\right) \quad (2)$$

In these equations, f is the frequency of AC signal, C_m is the cell membrane capacitance, and R is the radius of the cell. Based on these equations and reported parameters (C_m = 1.5 μf cm^{-2}, ρ_{int} = 4.5 Ω m, ρ_{ext} = 9 Ω m, and R = 1 μm),[35] the electrical field necessary to produce 1 V transmembrane potential required for bacteria cell membrane electroporation was calculated to be 10 kV cm^{-1}.

We plot the transmembrane potential as a function of frequency in Fig. 2A for the case of an applied electric field of 10 kV cm^{-1}. There is a modulation frequency window out to about 1 MHz over which the transmembrane potential can be maintained at a high level. We also used simulation to explore whether structuring of electrodes could dramatically increase the local electric field for a given AC applied bias. Fig. 2B shows the simplified structured electrodes schematic used for the electrical field simulation. These electrodes mimic the morphologies of the 3DSTEs, but given the complexity of the fractal structures, only represent an approximation. It is apparent from the model that the x–y plane demonstrates higher electrical field concentration near the sharp tips of the electrodes. The peak field of structured electrodes near the sharp tips showed hot spots of 20 kV cm^{-1} under the bias conditions we considered, but the planar electrodes field was limited to 8 kV cm^{-1} (data not shown).

We explored, *via* experiment, the role of modulation frequency and voltage in the efficiency of biomarker release, and also in achieving a low electrochemical current indicative of minimal hydroxyl generation. As seen in Fig. 3, by operating at 500 kHz, we were able to suppress by over one order of magnitude (compared to lower frequencies) the current associated with RNA-degrading radical production. To identify a boundary condition for electrical and electrochemical lysis, we measured the current generated at a voltage of 80 V_{pp} as a function of frequency. As shown in the inset to Fig. 3A, for any frequencies higher than 500 kHz, the current decreases by more than one order of magnitude while for lower frequencies, significant current is generated. We determined that 500 kHz represents an approximate boundary frequency between electrical and electrochemical lysis. While all frequencies greater than 500 kHz result in very low current, we opted to stay at 500 kHz to study electrical lysis as transmembrane potential drops dramatically when nearing 1 MHz (Fig. 3).

The original hypothesis behind the design of the 3DSTE device was that the sharp tips of the electrodes would create a strong electrical field that could not be achieved with planar electrodes. To investigate the role of the morphology of the 3DSTEs directly, we compared a set of planar electrodes *vs.* the 3DSTEs for an AC voltage of 80 V_{pp}. In Fig. 3C, results from flow cytometry trials are shown that evaluate the levels of propidium iodide taken up in the differently treated samples. Under these conditions, the uptake of the dye by bacteria processed using planar electrodes was essentially the same as for the case of the unprocessed (no field applied) control. In contrast, when 3DSTEs were employed, uptake consistent with complete lysis (*i.e.* comparable to a heat-lysed reference sample) was observed. These results confirm that the morphology of the 3DSTEs is a requisite feature of a device that can perform high-throughput electrical lysis.

We sought also to demonstrate that the flow rates of our system could provide clinically-relevant sample processing

speeds. The multi-channel devices we created achieved an aggregate sample processing rate of 50 μL min^{-1} combined with an electrical lysis efficiency of 95% (Fig. 3D). This corresponds to 1600 cells s^{-1}, notably higher than in prior reports.[11]

With conditions identified that triggered electrochemical *versus* electrical lysis, we performed studies to characterize the integrity of nucleic acids isolated from cells lysed using each method. As shown in Fig. 4, cells were subjected to conditions producing the different types of lysis. The rupture of the cells was confirmed using flow cytometry and growth of bacteria on agar plates. The RNA isolated from each sample was then analysed to extract a RNA integrity number (RIN). RIN evaluates the 23S to 16S rRNA ratio,[36] and translates it to a number between 1 and 10, where 10 correspond to the highest RNA quality. As seen in Fig. 4C, the RIN of RNA from a sample subjected to electrical lysis samples is excellent (RIN = 8.5), while the RNA is strongly degraded when electrochemical lysis and the RIN decreases (RIN = 4).

In order to further characterize the integrity of the nucleic acids released using electrical *versus* electrochemical lysis, we investigated quantitative PCR (qPCR) efficiencies for five reference genes specific to *E. coli* (Fig. 5). The RNA was isolated from the cells using both methods, reverse transcribed into DNA, and amplified. As shown in Fig. 5, there was a significant increase in the copy number of RNA transcripts (non-degraded RNA) available in electrically lysed *E. coli* cells in comparison to electrochemically lysed samples for all five genes as shown by the differences in the average Ct values (30.4 ± 0.2 and 24.5 ± 0.1 for electrochemical and electrical lysis methods, respectively). Thus, using electrical lysis instead of electrochemical lysis is preferred, especially when rare transcripts are analysed.

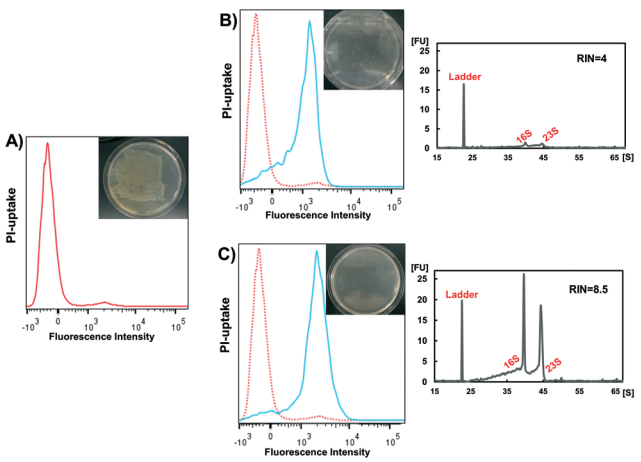

Fig. 4 Assessment of ribosomal RNA integrity in samples subjected to electrical and electrochemical lysis. A) Flow cytometry measurements and growth of unlysed bacteria. Flow cytometry measurements, growth of lysed bacteria, and RIN analysis for B) electrochemical lysis and C) electrical lysis. Red flow cytometry traces are control samples, while blue traces are subjected to conditions triggering electrical or electrochemical lysis. The conditions for electrochemical lysis are f = 50 kHz, V_{pp} = 60 V, and lysis rate = 800 cell s^{-1} and for electrical lysis are f = 500 kHz, V_{pp} = 80 V, and lysis rate = 800 cell s^{-1}.

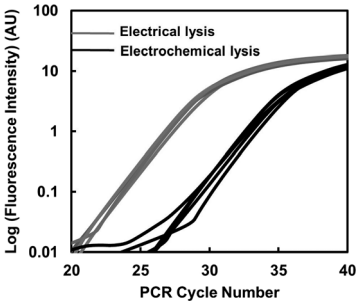

Fig. 5 Evaluation of mRNA integrity by PCR. Analysis of qPCR efficiency for five E. coli RNA transcripts in cells lysed using electrical (grey) or electrochemical (black) treatment. Higher copy numbers judged by increased signal at lower cycle numbers were consistently observed with electrical lysis.

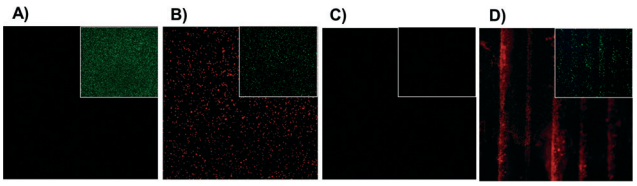

Fig. 6 Investigation of electroporation *versus* complete rupture using electrical lysis (D) *versus* thermal (B) or chemical treatment (C). Panel (A) depicts signals obtained with untreated *E. coli*. *E. coli* expressing GFP (green channel, inset) were incubated with propidium iodide (red channel, large images). For the electrical lysis, signals consistent with electroporation, and not complete cell rupture are obtained (positive for both red and green fluorescence).

The electrical lysis process described could, in principle, be liberating biomarkers from the cells *via* transient electroporation of the cell wall or complete rupture. To investigate the extent of lysis, we used GFP bacteria incubated with propidium iodide (PI) i) before and after processing with our device under concentrated electrical field condition (Fig. 6D), ii) after lysis with NaOH (Fig. 6C), and iii) after lysis at high temperatures (Fig. 6B). If bacteria are permeabilized, PI can diffuse inside the cell *via* the pores and intercalate into DNA, which then emits red fluorescence. The bacteria will retain their green fluorescence only if their membrane is not completely ruptured. Fig. 6 shows fluorescent imaging of bacteria before and after lysis. In the case of thermal lysis, the cells fluorescence both red and green confirming that bacterial membranes have been permeated, but not lysed. However, when bacteria are completed lysed using NaOH, they burst and cells are no longer intact or present. After processing with our device using electrical lysis conditions, bacteria have both red and green fluorescence demonstrating that, using electrical lysis in our device, the bacteria are indeed electroporated and not lysed.

Conclusions

We have described a microfluidic device for the preparation of samples for subsequent molecular bioanalysis. The approach

leverages three-dimensional, sharp-tipped gold electrodes created using electrodeposition to generate a high local electric field at sharp tips. This allowed us to operate at practical voltages, and also at AC modulation frequencies at which a vastly lower rate of current, and thus radical production, was achieved. These advantages combined led to a high-throughput biomarker extraction device that preserves the integrity of biomarkers to be analysed, such as RNA.

Acknowledgements

We acknowledge Dr. Brian Lam and Justin Besant for their advice throughout this project. We also acknowledge the use of Toronto Nanofabrication Centre (TNFC) facilities. NSERC, the Ontario Research Fund (Research Excellence), and CIHR (Emerging Team Grant) are also acknowledged.

Notes and references

1 D. R. Walt, *Science*, 2005, **308**, 217–219.
2 N. L. Rosi and C. A. Mirkin, *Chem. Rev.*, 2005, **105**, 1547–1562.
3 P. Yager, T. Edwards, E. Fu, K. Helton, K. Nelson, M. R. Tam and B. H. Weigl, *Nature*, 2006, **442**, 412–418.
4 J. Kim, J. W. Hong, D. P. Kim, J. H. Shin and I. Park, *Lab Chip*, 2012, **12**, 2914–2921.
5 J. Kim, M. Johnson, P. Hill and B. K. Gale, *Integr. Biol.*, 2009, **1**, 574–586.
6 D. Di Carlo, C. Ionescu-Zanetti, Y. Zhang, P. Hung and L. P. Lee, *Lab Chip*, 2005, **5**, 171–178.
7 J. T. Nevill, R. Cooper, M. Dueck, D. N. Breslauer and L. P. Lee, *Lab Chip*, 2007, **7**, 1689–1695.
8 H. J. Lee, J.-H. Kim, H. K. Lim, E. C. Cho, N. Huh, C. Ko, J. C. Park, J.-W. Choi and S. S. Lee, *Lab Chip*, 2010, **10**, 626–633.
9 S. M. McKenna and K. J. Davies, *Biochem. J.*, 1988, **254**, 685–692.
10 D. Di Carlo, K.-H. Jeong and L. P. Lee, *Lab Chip*, 2003, **3**, 287–291.
11 G. Mernier, N. Piacentini, T. Braschler, N. Demierre and P. Renaud, *Lab Chip*, 2010, **10**, 2077–2082.
12 B. Lam, Z. Fang, E. H. Sargent and S. O. Kelley, *Anal. Chem.*, 2012, **84**, 21–25.
13 H.-Y. Wang, A. K. Bhunia and C. Lu, *Biosens. Bioelectron.*, 2006, **22**, 582–588.
14 H. Lu, M. A. Schmidt and K. F. Jensen, *Lab Chip*, 2005, **5**, 23–29.
15 E. J. Menke, M. A. Thompson, C. Xiang, L. C. Yang and R. M. Penner, *Nat. Mater.*, 2006, 914–918.
16 B. J. Plowman, S. K. Bhargava and A. P. O'Mullane, *Analyst*, 2011, **136**, 5107–5119.
17 S. E. Brunker, K. B. Cederquist and C. D. Keating, *Nanomedicine*, 2007, **2**, 695–710.
18 D. Bera, S. C. Kuiry and S. Seal, *JOM*, 2004, **56**, 49–53.
19 D. Bera, S. C. Kuiry, S. Patil and S. Seal, *Appl. Phys. Lett.*, 2003, **82**, 3089–3092.
20 G. Fasol and K. Runge, *Appl. Phys. Lett.*, 1997, **70**, 2467–2468.
21 D. Wang, W. L. Zhou, B. F. McCaughy, J. E. Hampsey, X. Ji, Y.-B. Jiang, H. Xu, J. Tang, J. H. Schmehl, C. O'Connor, C. J. Brinker and Y. Lu, *Adv. Mater.*, 2003, **15**, 130–133.
22 Y. Huang, Y. Yamauchi, C. Lai and W. Chen, *J. Hazard. Mater.*, 2013, DOI: 10.1016/j.jhazmat.2013.10.054.
23 L. Soleymani, Z. Fang, B. Lam, X. Bin, E. Vasilyeva, A. J. Ross, E. H. Sargent and S. O. Kelley, *ACS Nano*, 2011, **5**, 3360–3366.
24 K. Zhou, L. Zhou, Q. Lim, R. Zou, G. Stephanopoulos and H. Too, *BMC Mol. Biol.*, 2011, 18.
25 L. Soleymani, Z. Fang, E. H. Sargent and S. O. Kelley, *Nat. Nanotechnol.*, 2009, **4**, 844–848.
26 B. Lam, J. Das, R. D. Holmes, L. Live, A. Sage, E. H. Sargent and S. O. Kelley, *Nat. Commun.*, 2013, **4**, 2001.
27 J. D. Besant, J. Das, E. H. Sargent and S. O. Kelley, *ACS Nano*, 2013, **7**, 8183–8189.
28 L. Soleymani, Z. Fang, X. Sun, H. Yang, B. J. Taft, E. H. Sargent and S. O. Kelley, *Angew. Chem., Int. Ed.*, 2009, **48**, 8457–8460.
29 I. Ivanov, J. Stojcic, A. Stanimirovic, E. Sargent, R. K. Nam and S. O. Kelley, *Anal. Chem.*, 2013, **85**, 398–403.
30 H. Yang, A. Hui, G. Pampalakis, L. Soleymani, F.-F. Liu, E. H. Sargent and S. O. Kelley, *Angew. Chem., Int. Ed.*, 2009, **48**, 8461–8464.
31 E. Vasilyeva, B. Lam, Z. Fang, M. D. Minden, E. H. Sargent and S. O. Kelley, *Angew. Chem., Int. Ed.*, 2011, **50**, 4137–4141.
32 J. Das and S. O. Kelley, *Anal. Chem.*, 2011, **83**, 1167–1172.
33 A. Bhimji, A. Zaragoza, L. S. Live and S. O. Kelley, *Anal. Chem.*, 2013, **85**, 6813–6819.
34 J. Das, K. B. Cederquist, A. A. Zaragoza, P. E. Lee, E. H. Sargent and S. O. Kelley, *Nat. Chem.*, 2012, **4**, 642–648.
35 W. Bai, K. S. Zhao and K. Asami, *Biophys. Chem.*, 2006, **122**, 136–142.
36 A. Schroeder, O. Mueller, S. Stocker, R. Salowsky, M. Leiber, M. Gassmann, S. Lightfoot, W. Menzel, M. Granzow and T. Ragg, *BMC Mol. Biol.*, 2006, **7**, 3.

